Phonons and Crystal Field Levels in Dysprosium Garnets by Raman Scattering*

R. L. Wadsack, Joan L. Lewis, B. E. Argyle,† and R. K. Chang
Becton Center, Yale University, New Haven, Connecticut 06520
(Received 20 January 1971)

Raman scattering from DyAl and DyGa garnets at 80 K was investigated to determine the Raman-active phonons ($3A_{1g}+8E_g+14T_{2g}$) and the $^6H_{15/2}$ and $^6H_{13/2}$ crystal field levels. The frequencies and the symmetries of all the Raman-active phonons in DyGa garnets and all except one phonon in DyAl garnets were determined. The positions of the lowest four levels in the $^6H_{15/2}$ manifold and all seven levels in the $^6H_{13/2}$ manifold were measured in DyAl and DyGa garnets. For DyAl garnets, the $^6H_{13/2}$ manifold has hitherto not been observed. A full crystal field calculation was carried out using our Raman data on the $^6H_{15/2}$ and $^6H_{13/2}$ manifolds along with the absorption data of Grünberg *et al.* and of Aoyagi *et al.* on the other higher-energy crystal field levels. The crystal field Hamiltonian appropriate for the D_2 symmetry of the rare-earth sites was used, and the mixing of the different J states by the crystal field was included. The best-fit values for the nine crystal field parameters plus the free-ion energies were found. These values were similar to those obtained by Grünberg *et al.* for the dilute garnets YAlG (Dy) and YGaG(Dy). The relative electronic Raman intensities, measured for our selected combinations of incident and scattered polarizations, are listed. It is shown how these intensities are related to the Raman-scattering tensors, which in turn depend on the crystal field eigenfunctions. In principle, the Raman intensity ratios can provide a good test of the crystal field analysis, analogous to the role of the g tensor.

I. INTRODUCTION

Dysprosium aluminum garnet (DyAlG) and dysprosium gallium garnet (DyGaG) belong to a large class of materials which have the general formula $3R_2O_3 \cdot 5A_2O_3$, where R represents a rare-earth ion or yttrium, and A represents aluminum, gallium, or iron. Limited attention has been given to the lattice spectra of the garnets, perhaps because of their complicated crystal structure. The garnet space group is O_h^{10},[1] one of the most complicated groups, with 48 operations in the point group and eight different nonprimitive translations.[2] Recently McDevitt[3] has reported on the infrared phonon spectra of a large number of rare-earth garnets. Reports on the Raman phonon spectra of garnets have also been recent and limited.[4,5]

In contrast to the lattice spectra, the electronic spectra of the rare-earth garnets have received a great deal of attention. In particular, rare-earth ions in a diamagnetic environment (paramagnetic garnets where A is aluminum or gallium) have received the most attention for three reasons. First, they provide efficient solid-state lasers.[6,7] Second, crystal field analyses can be applied to their electronic spectra.[8] Third, they serve as a necessary intermediary to the eventual understanding of the rare-earth iron garnets, where the competing effect of a large exchange interaction is present. Of the paramagnetic garnets, DyAlG has received the most attention. This is because below its Néel temperature $T_N = 2.49$ K it can be very well described by an Ising model.[9] The optical spectra of the dysprosium garnets have recently been reported by Grünberg *et al.*[10] and by Aoyagi *et al.*[11] Common to both their work was the absence of any data on the crystal field levels of the $^6H_{13/2}$ manifold in DyAlG and DyGaG. Furthermore, only a few of the crystal field levels of the ground-state manifold $^6H_{15/2}$ have been observed. The lack of such experimental data discouraged Grünberg *et al.*[10] from performing a complete crystal field analysis on DyAlG and DyGaG. Instead, such analyses were performed on dilute salts of YAlG (Dy) and YGaG (Dy), where the absorption data were supplemented by fluorescence data. Besides these crystals, the only other complete and satisfactory treatment of crystal field interaction is for YAlG (Yb) and YGaG (Yb).[12]

The apparatus used in this work is discussed in Sec. II. The Raman-active phonon frequencies and their symmetries are found in Sec. III. Section IV presents the energies of the $^6H_{15/2}$ and $^6H_{13/2}$ levels, as determined by electronic Raman scattering. The crystal field analyses and results for DyAlG and DyGaG are also presented in Sec. IV. The relative electronic Raman intensities for different incident and scattered polarizations are listed in Sec. V. The relation of these intensities to the Raman-scattering tensors, which in turn depend on the eigenfunctions of each crystal field level, is also given in Sec. V.

II. APPARATUS

The excitation source used in this Raman-scattering experiment was a flowing-gas argon laser.[13] Data were taken both with the 4880- and the 5145-Å laser emissions (approximately $\frac{1}{3}$ W each), in order

to eliminate misidentification of our Raman data due to possible fluorescence from trace impurities. Single crystals of DyAlG and DyGaG (flux grown) were x-ray oriented, but into parallel solids, polished, and mounted in a "cold-finger" liquid-nitrogen Dewar. The sizes of the DyAlG and DyGaG used were $2.3\times2.8\times3.6$ mm^3 and $2.0\times3.8\times5.6$ mm^3, respectively. The longest dimension of each was parallel to the incident laser direction. The sample temperature was estimated to be 80 K from the Stokes and anti-Stokes ratio of a phonon. The tandem spectrometer Spex 1400 II had two gratings of 600 grooves/mm blazed for 7500 Å. A polarization scrambler from Spex was used so that the spectrometer's transmission characteristic would be insensitive to polarizations of the scattered radiation. This facilitated the determination of the Raman intensities for various combinations of incident and scattered radiation, pertaining especially to the discussion in Sec. V. The photomultiplier EMI 9558 A was cooled to $-20\,^{\circ}$C as well as magnetically focused (EMI Magnetic Lens Assembly MLO + M1) in order to significantly reduce the dark counts. A digital photon counter[14] processed the photomultiplier output in such a way that its analog output was proportional to the photomultiplier count rate *normalized* to the incident laser intensity, which was continuously monitored by a photodiode EGG SGD-100. Consequently, both short-term fluctuations and long-term drifts of the laser were automatically accounted for in our Raman data. The normalized analog output of the photon counter was displayed on a recorder.

III. PHONONS

The crystal structures of DyAlG and DyGaG belong to the space group O_h^{10} ($Ia3d$), and are isomorphic to YAlG. The $K\approx0$ phonons of these garnets can be classified according to their symmetry properties by the irreducible representations of the factor group.[15] Hurrell *et al.*[4] have performed such a factor-group analysis for YAlG and found that the total irreducible representations of the transverse optical modes are

$$\Gamma = 18T_{1u} + 3A_{1g} + 8E_g + 14T_{2g} + 5A_{2g} + 5A_{1u} + 5A_{2u} + 10E_u + 14T_{1g} + 16T_{2u}\,. \quad (1)$$

Most of the infrared-active phonons (T_{1u}) for a large number of rare-earth ions in aluminum, gallium, and iron garnets have been reported by McDevitt.[3] Some of the Raman-active phonons (A_{1g}, E_g, T_{2g}) in DyAlG have been reported by Mace *et al.*[5]

The Raman-scattering intensity due to phonons depends on the polarizations of the incident and scattered radiation with respect to the crystal axes. Such dependencies can be summarized by making use of the scattering matrices given by Loudon[16] for all the phonon modes. Raman scattering resulting from the A_{1g}, E_g, and T_{2g} phonons can be readily distinguished if a judicial choice is made for the polarization directions and the macroscopic crystal axes. In our experiment, the incident and right-angle scattered light directions were parallel within 5° to the [110] and the [$\bar{1}$10] crystal axes, respectively. These directions are in the laboratory horizontal plane, thus making the crystal [001] axis vertical. The notation *V-V*, *H-H*, *V-H*, and *H-V* will be used throughout this paper to designate incident-polarization-scattered polarization as being in the horizontal plane *H* or vertical plane *V*.

With such a choice of crystal orientation, each phonon mode does scatter in at least one polarization combination, and does not scatter for at least one other such combination. In particular, for *H-H*, only the E_g modes will scatter, while for *V-H* and *H-V* only the T_{2g} modes will scatter. In the *V-V* combination both the E_g and A_{1g} will scatter. Thus, the symmetry of the phonons is readily determined by the presence and absence of Raman scattering for various polarization combinations. If the crystal were oriented in a less optimal direction, the Raman intensities for different polarization combinations would often be quite similar, and therefore detailed comparisons between theoretical and experimental intensity ratios would be necessary in order to identify the mode. Typical experimental data for DyAlG and DyGaG at 80 K are shown in Figs. 1 and 2, respectively. One notes that the observed Raman spectra for phonons obey well the selection rules dictated by Loudon's scattering matrices.[16] In fact, the residual intensities of the A_{1g} modes in the "forbidden" polarization combinations (*H-H*, *V-H*, and *H-V*) were found to be less than 0.5% of the intensities in the "allowed" polarization combination (*V-V*). For the T_{2g} and E_g modes, the residual intensities were found to be less than 5 and 1%, respectively, of the intensities in the "allowed" polarization combinations. This is to be expected, because the scattering matrices of the A_{1g} modes are diagonal, and those of the T_{2g} and E_g modes are not. Consequently, the T_{2g} and E_g modes should be more sensitive than the A_{1g} modes to the accuracy of the crystal alignment (within 5° for our case) and to the finite solid angle of the collection optics for the scattered light (approximately $\frac{1}{2}f$).

The frequencies and symmetries of the observed Raman-active phonons in DyAlG and DyGaG at 80 K are listed in Table I. All the $K\approx0$ Raman-active phonons have been observed in DyGaG, while all but one E_g mode have been observed in DyAlG. The relative scattering efficiencies of these phonons for unpolarized incident and scattered radiations $I_{U\text{-}U}$ are listed beside the phonons to indicate their relative strengths.

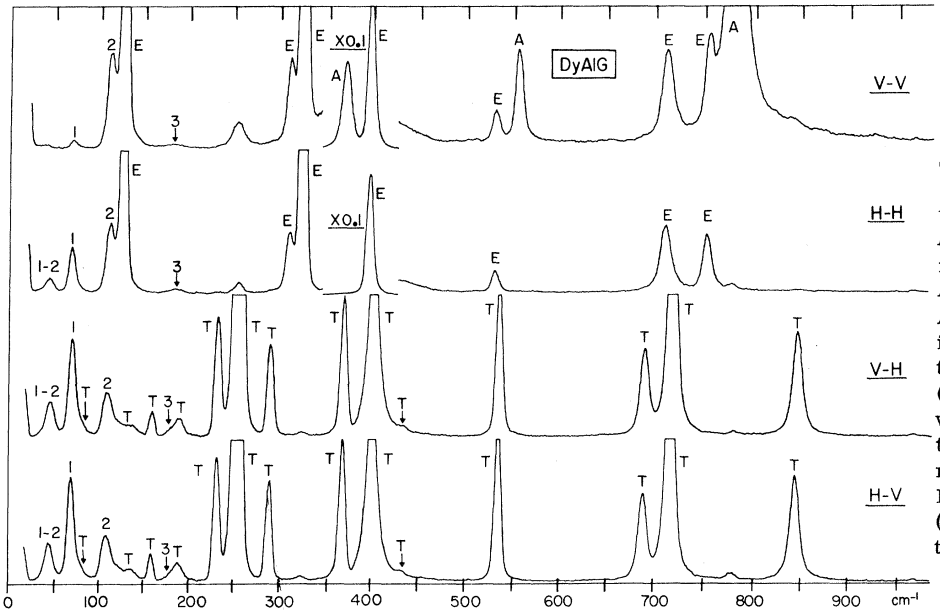

FIG. 1. Experimental Raman spectra of oriented single crystal of DyAlG at 80 K measured for four combinations of incident and scattered polarizations *V-V*, *H-H*, *V-H*, and *H-V* (see text). $K \approx 0$ Raman-active phonons A_{1g}, E_g, and T_{2g} (labeled as A, E, T) and the electronic Raman transitions among the $^6H_{15/2}$ crystal field levels (labeled as 1, 2, 3 and 1-2) were identified using the polarization selection rules for Raman scattering. For energies, see Table I (phonons) and Table II (electronic levels).

IV. CRYSTAL FIELD LEVELS

The most complete study of the crystal field levels in DyAlG and DyGaG has been that of Grünberg *et al.*[10] By optical-absorption techniques, they were able to assign most of the energy levels for the ^6H and ^6F multiplets. Their assignments were in fair agreement with those determined by Aoyagi *et al.*[11] for DyAlG and by Veyssie and Dreyfus[17] for DyGaG. Characteristic of all the previous work was the complete lack of experimental data for the $^6H_{13/2}$ manifold and the partial lack of data for the ground-state $^6H_{15/2}$. Since the energies of both these manifolds are within the capabilities of our Raman apparatus, electronic Raman scattering[18] in DyAlG and DyGaG was attempted. However, as the energies of the $^6H_{15/2}$ manifold occur in the same region as the Raman-active phonon energies, a complete knowledge of the phonon assignments takes on a special significance. The fact that the symmetry and frequency of all the phonons in DyAlG and all but one in DyGaG are now known (see Sec. III) assures that any additional Raman peaks can be attributed to the rare-earth electronic levels.

All of the seven crystal field levels in $^6H_{13/2}$ and only the lowest four levels of the $^6H_{15/2}$ manifold were observed for both crystals. Table II summarizes these results. The unprimed numbers designate states of the ground manifold $^6H_{15/2}$, and the primed numbers designate states of the first excited manifold $^6H_{13/2}$. A single numeral, for example, 3, indicates an electronic Raman transition from the ground state 0 to the excited state 3. Double numerals, for example, 1-0′, indicate a Raman transition from the state 1 (first excited level in the ground manifold) to the state 0′ (the bottom level of the $^6H_{13/2}$ manifold). Note the transitions originating from the first two excited levels of $^6H_{15/2}$, which were observable because the crystals were at 80 K. This, in fact, gives us

TABLE I. Species (A_{1g}, E_g, T_{2g}) and corresponding energies (cm^{-1}) of the Raman-active phonons measured at 80 K for DyAlG and DyGaG. Their scattering strengths I_{U-U} for unpolarized radiations are also listed.

DyAlG				DyGaG		
Species	This work (cm^{-1})	I_{U-U}	Ref. (5) (cm^{-1})	Species	This work (cm^{-1})	I_{U-U}
T_{2g}	80±3	0.4	···	T_{2g}	87±3	0.4
E_g	130±3	13	···	E_g	99±3	0.5
T_{2g}	139±3	0.3	···	E_g	110±3	7.3
T_{2g}	164±3	1.0	162	T_{2g}	119±3	1.3
T_{2g}	194±3	0.7	···	T_{2g}	152±3	0.7
T_{2g}	237±3	4.5	234	U[a]	157±3	0.3
T_{2g}	259±3	27	259	T_{2g}	168±3	11
T_{2g}	292±3	3.4	292	T_{2g}	179±3	18
E_g	312±3	2.4	···	T_{2g}	238±3	25
E_g	324±3	17	325	E_g	258±3	17
T_{2g}	368±3	5.0	···	T_{2g}	271±3	16
A_{1g}	370±3	16	366	E_g	295±3	3.3
E_g	396±3	51	396	A_{1g}	350±3	44
T_{2g}	400±3	6.8	396	E_g	357±3	120
T_{2g}	431±3	0.1	···	T_{2g}	386±3	5.2
E_g	534±3	0.9	···	T_{2g}	414±3	2.7
T_{2g}	538±3	5.6	545	E_g	426±3	6.1
A_{1g}	558±3	1.6	564	T_{2g}	496±3	0.3
T_{2g}	688±3	3.0	693	T_{2g}	513±3	0.4
E_g	710±3	2.7	···	A_{1g}	527±3	28
T_{2g}	716±3	9.9	718	T_{2g}	594±3	20
E_g	753±3	2.3	757	T_{2g}	608±3	23
A_{1g}	781±3	25	790	E_g	635±3	1.1
T_{2g}	849±3	3.8	854	E_g	688±3	0.3
				T_{2g}	752±3	17
				A_{1g}	753±3	53
Total observed: $14T_{2g}$, $7E_g$, $3A_{1g}$				Total observed: $14T_{2g}$, $8E_g$, $3A_{1g}$		

[a]Unassigned.

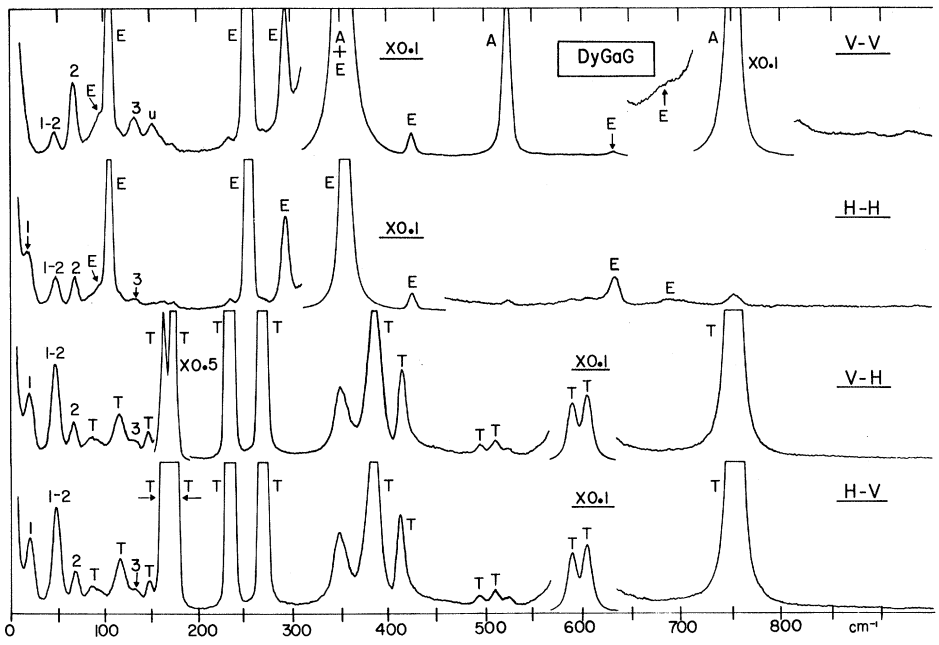

FIG. 2. Same as Fig. 1 except the oriented single crystal was DyGaG.

another means of determining the energies of levels 1 and 2 in $^6H_{15/2}$. The experimental Raman spectra for the $^6H_{15/2}$ crystal field levels of DyAlG and DyGaG are shown in Figs. 1 and 2, respectively, while those for the $^6H_{13/2}$ levels are shown in Figs 3 and 4. The relative Raman intensities for the different sets of polarizations are listed in Table II. Their significance in terms of testing the

TABLE II. Energies (cm^{-1}) of the observed electronic Raman transitions among the $^6H_{15/2}$ and $^6H_{13/2}$ manifolds. Relative intensities for all polarization combinations are listed.

		DyAlG (80 K)						DyGaG (80 K)				
Assignments		E (cm^{-1})	I_{V-V}	I_{H-H}	I_{V-H}	I_{H-V}	I_{U-U}	E (cm^{-1})	I_{V-V}	I_{H-H}	I_{V-H}	I_{H-V}	I_{U-U}
$^6H_{13/2}$	6′	3968	• • •	• • •	0.010	0.008	0.023	3824	• • •	• • •	0.024	0.020	0.044
	5′	3832	0.046	0.050	0.050	0.048	0.195	3784	0.012	0.014	0.012	0.012	0.050
	4′	3786	0.040	0.033	0.057	0.054	0.184	3747	0.035	0.027	0.049	0.046	0.156
	3′	3719[a]	0.089	0.058	0.065	0.068	0.28	3648	• • •	• • •	~0.070	~0.060	~0.130
	2′	3673	0.046	0.027	0.088	0.088	0.25	3635	~0.032	~0.025	~0.088	~0.098	~0.242
	1′	3594[b]	0.217	0.155	0.357	0.375	1.10	3576	0.48	0.40	0.49	0.48	1.85
	0′	3565	0.009	0.088	0.76	0.76	1.62	3559[c]	0.088	0.145	0.64	0.65	1.52
$^6H_{15/2}$	3	186	0.05	0.08	0.08	0.08	0.3	137	0.40	0.10	0.15	0.15	0.75
	2	114	1.7	1.3	0.8	0.8	4.6	70	1.2	0.50	0.50	0.50	2.7
	1	69	0.15	0.85	2.0	2.0	5.0	21	• • •	0.80	1.1	1.1	≥3
	0	0	• • •	• • •	• • •	• • •	• • •	0	• • •	• • •	• • •	• • •	• • •
	1-2	46	• • •	0.25	0.7	0.7	1.7	49	0.40	0.55	1.7	1.7	4.3
	1-6′	3898	0.003	• • •	• • •	• • •	0.003	3803	0.010	• • •	• • •	• • •	0.010
	1-5′	3762	0.005	0.006	0.013	0.011	0.036	3764	0.007	0.006	0.016	0.005	0.034
	1-4′	• • •	• • •	• • •	• • •	• • •	• • •	3726	0.012	0.010	0.018	0.016	0.056
	1-3′	3649	0.010	0.010	0.027	0.026	0.074	3627	~0.058	~0.039	~0.10	0.10	~0.30
	1-2′	• • •	• • •	• • •	• • •	• • •	• • •	3614	~0.014	~0.005	~0.021	0.028	~0.068
	1-1′	3524	0.005	0.015	0.088	0.088	0.195	• • •	• • •	• • •	• • •	• • •	• • •
	1-0′	3498	0.268	0.21	0.088	0.088	0.653	3540	0.41	0.36	0.27	0.27	1.31
	2-1′	3481	0.033	0.031	0.007	0.006	0.077	3506	0.005	0.008	0.040	0.042	0.095
	2-0′	• • •	• • •	• • •	• • •	• • •	• • •	3491	0.005	• • •	0.009	0.010	0.023

[a]Intensity contains some 1-4′.

[b]Intensity contains some 1-2′.

[c]Intensity contains some 1-1′.

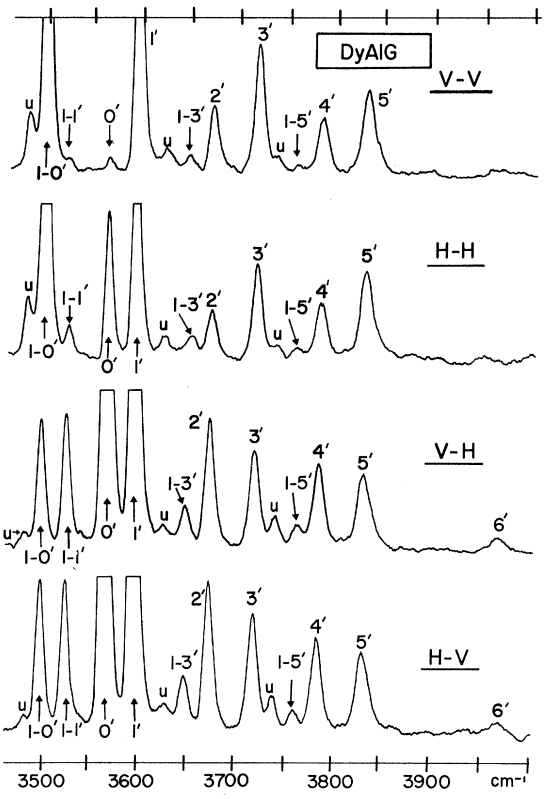

FIG. 3. Experimental electronic Raman spectra of DyAlG at 80 K measured for four combinations of incident and scattered polarizations *V-V*, *H-H*, *V-H*, and *H-V* (see text). Electronic Raman transitions are between the ground $^6H_{15/2}$ manifold and the upper $^6H_{13/2}$ manifold. Single prime numerals designate transitions from the ground state to the various levels (0′, 1′, . . ., 6′) of the $^6H_{13/2}$ manifold. Double numerals indicate Raman transitions from excited levels of $^6H_{15/2}$ ground manifold (1, 2, . . ., 7) to the various $^6H_{13/2}$ levels. Letter "u" designates unassigned peaks. For energies see Table II.

quality of the crystal field analysis will be discussed in Sec. V.

Some previous work on the electronic Raman scattering involving the $^6H_{15/2}$ manifold of DyAlG has been reported by Mace *et al.*[5] and by Koningstein and Ng.[19] Their results were inconsistent with each other and are in poor agreement with our work.

Crystal field calculations involving the full Hamiltonian appropriate for the D_2 symmetry at the rare-earth sites and including the mixing of the different J states by the crystal field were performed by Grünberg *et al.*[10] only for dysprosium doped in YAlG and in YGaG. This is because the energy assignments in the dilute salts are much more complete than for the pure garnets, for which the absorption data cannot be supplemented by fluorescence data. Our new assignments in the $^6H_{15/2}$ and $^6H_{13/2}$ manifolds, in addition to the previous assignments by Grünberg *et al.* for all the other higher-energy manifolds, motivated us to perform a crystal field calculation for DyAlG and DyGaG similar to that done for the dilute salts.

The crystal field calculations were done using the Stevens[20] form of the Hamiltonian for D_2 symmetry,

$$H = A_0^2\langle r^2\rangle V_0^2 + A_2^2\langle r^2\rangle V_2^2 + A_0^4\langle r^4\rangle V_0^4 + A_2^4\langle r^4\rangle V_2^4 + A_4^4\langle r^4\rangle V_4^4 + A_0^6\langle r^6\rangle V_0^6 + A_2^6\langle r^6\rangle V_2^6 + A_4^6\langle r^6\rangle V_4^6 + A_6^6\langle r^6\rangle V_6^6 . \quad (2)$$

The matrix elements for the V_q^k are related to the tensor operators U_q^k by

$$(f^n\gamma SLJJ_z|\, V_q^k | f^n\gamma' SL'J'J_z') = N_q^k (f^n\gamma SLJJ_z|\, U_q^k | f^n\gamma' SL'J'J_z') , \quad (3)$$

where the coefficients N_q^k are given in Dieke.[21]

The matrix elements of the tensor operators U_q^k are given by the relations

$$(f^n\gamma SLJJ_z|\, U_q^k | f^n\gamma' SL'J'J_z') = (-1)^{J-M} \begin{pmatrix} J & k & J' \\ -J_z & q & J_z' \end{pmatrix} \times (f^n\gamma SLJ \| U^k \| f^n\gamma' SL'J') , \quad (4)$$

$$(f^n\gamma SLJ \| U^k \| f^n\gamma' SL'J') = (-1)^{S+L'+J+k} \times [(2J+1)(2J'+1)]^{1/2} \begin{Bmatrix} L & J & S \\ J' & L & k \end{Bmatrix} \times (f^n\gamma SL \| U^k \| f^n\gamma' SL') , \quad (5)$$

where the reduced matrix elements $(SL\|U^k\|SL')$ have been calculated by Nielson and Koster.[22]

To find the best fit of the calculated crystal field energies to the experimental energies, a modified least-squares procedure of Powell[23] was used. The 12 free-ion energies and the nine crystal field parameters were used as variables. The program used in this paper was checked by reproducing the results of Grünberg *et al.* for dysprosium doped in YAlG, using Wybourne's free-ion energies[24] and the Hutchings and Wolf crystal field parameters as starting values. Table III, column (A) gives the best-fit results of Grünberg *et al.* with the above starting values. Column (B) gives our results using these same starting values. Column (C) gives our results using column (A) as starting values. Note that columns (B) and (C) have the same rms error (shown in the last row) on the energy discrepancies, but have slightly different final values for some of the free-ion energies and crystal field parameters.

In the crystal field calculation for DyAlG and DyGaG, the starting values were those of the dilute garnets shown in columns (C) and (E), respectively. Our best-fit values for the free-ion assignments

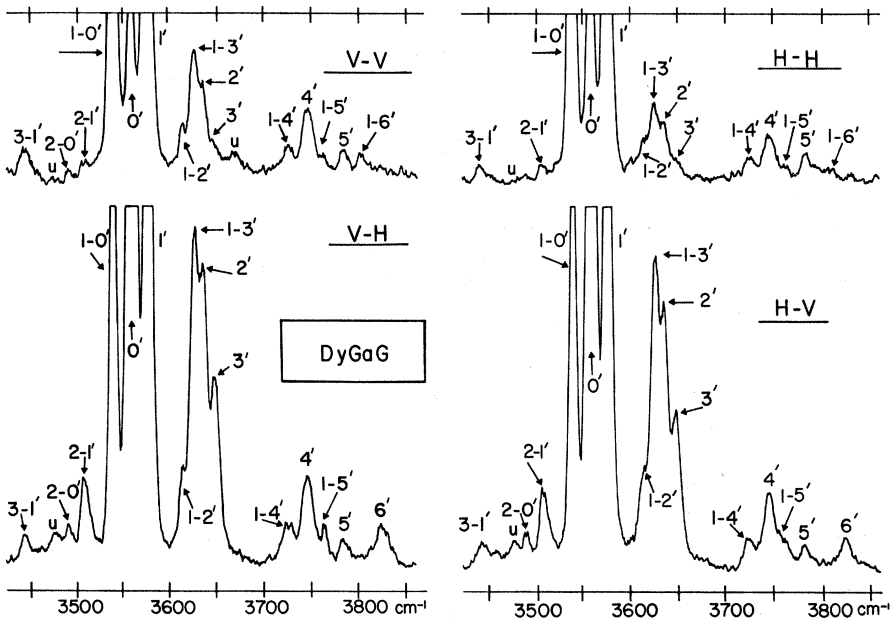

FIG. 4. Same as Fig. 3 except the single crystal was DyGag.

TABLE III. Free-ion assignments (cm^{-1}) and crystal field parameters. See text for description of columns.

Free-ion assignment	Ref. 24	YAlG(Dy) Ref. 10 (A)	YAlG(Dy) This work (B)	This work (C)	DyAlG This work (D)	YGaG(Dy) Ref. 10 (E)	DyGaG This work (F)	DyGaG Ref. 17 (G)	DyGaG This work (H)
$^6F_{1/2}$	13 843	• • •	13 098	13 098	13 080	• • •	13 109		13 080
$^6F_{3/2}$	13 299	12 985	12 984	12 983	12 988	12 994	12 992		12 996
$^6F_{5/2}$	12 550	12 189	12 185	12 185	12 189	12 198	12 200		12 200
$^6F_{7/2}$	11 130	10 796	10 791	10 790	10 794	10 804	10 807		10 809
$^6H_{5/2}$	10 089	10 080	10 077	10 076	10 077	10 079	10 079		10 074
$^6F_{9/2}$	9 164	8 918	8 910	8 911	8 917	8 927	8 930		8 934
$^6H_{7/2}$	9 033	8 983	8 984	8 983	8 993	8 976	8 975		8 965
$^6F_{11/2}$	7 920	7 570	7 561	7 560	7 571	7 555	7 557		7 552
$^6H_{9/2}$	7 613	7 614	7 619	7 620	7 623	7 625	7 622		7 628
$^6H_{11/2}$	5 778	5 761	5 759	5 759	5 755	5 764	5 766		5 763
$^6H_{13/2}$	3 457	3 446	3 445	3 447	3 440	3 447	3 447		3 441
$^6H_{15/2}$	0	0	0	0	0	0	0		0
Crystal field parameters									
$A_0^2\langle r^2\rangle$		−170	−170	−169	−183	−22	−34	87	71
$A_2^2\langle r^2\rangle$		334	332	328	309	141	192	162	175
$A_0^4\langle r^4\rangle$		−292	−297	−298	−305	−282	−274	−235	−264
$A_2^4\langle r^4\rangle$		240	251	267	213	181	195	215	138
$A_4^4\langle r^4\rangle$		1046	1065	1066	1120	1040	985	945	1032
$A_0^6\langle r^6\rangle$		41	42	42	44	36	37	67	35
$A_2^6\langle r^6\rangle$		−142	−138	−131	−151	−108	−104	−10	−113
$A_4^6\langle r^6\rangle$		747	735	734	688	725	681	902	688
$A_6^6\langle r^6\rangle$		−77	−85	−80	−119	−57	−93	−200	−164
rms error		6.5	5.6	5.6	6.6	7.2	6.6	• • •	7.8

and the crystal field parameters are shown in column (D) for DyAlG and column (F) for DyGaG. It is of interest to note that both sets of values for the dysprosium garnets are very similar to those for the dilute salts.

The crystal field parameters shown in columns (D) and (F) are quantized along the same local axes as those for the dilute salts discussed by Grünberg *et al.* The g_z axis is along the η or ζ local axis. In order to obtain the large g_z for the ground state in DyAlG, one needs to rotate either the axes or crystal field parameters shown in Table III by 90° about the η or ζ axes.

Veyssie and Dreyfus[17] also did a crystal field analysis for DyGaG, with results shown in column (G). Using their results as starting values in our program, the values in column (H) were obtained. There is a substantial difference between the two sets of crystal field parameters [see columns (F) and (H)]. Judging from their similar rms errors (shown in the last row), we did not feel justified in preferring the values in column (E) over those in column (H). It was thought that the two sets of crystal field parameters were related by ±90° or ±180° about the local axes (ξ, η, ζ) but this proved not to be the case. We thus concluded that using the least-squares-fit procedure of Powell, the computer was not able to reach the lower rms error minimum [column (F)] but found instead a local minimum [column (H)], which had a larger rms error.

Table IV shows the comparison of the calculated crystal field energies and the observed energies. The differences between these are shown for convenience. For the observed energies, our Raman results were used for the $^6H_{15/2}$ and $^6H_{13/2}$ manifolds, while the data of Grünberg *et al.* and of Aoyagi *et al.* were used for the remaining levels.

V. RELATIVE INTENSITIES

Up to now, the relative intensities in the Raman spectra were used, insofar as their presence and absence for a given polarization combination, to determine the symmetry of the phonons (see Sec. III). This section will discuss the relative intensities of the electronic Raman lines, which were measured for our polarization combinations. In addition, we will discuss how these intensities might be used to gain information about how the crystal field interaction mixes the pure spin-orbit states of the trivalent rare-earth ions situated in a site with D_2 symmetry.

The intensity associated with a Raman transition between states β and β', which are specified by "free-ion" Russell-Saunders coupled wave functions $|\gamma SLJJ_z\rangle$, has been derived by Axe[25] and by Mortenson and Koningstein,[26] using the closure relation of Judd[27] and Ofelt,[28] in terms of the electronic Raman-scattering tensor $(\alpha_{\rho\sigma})_{\beta'\beta}$. Here ρ and σ denote the polarization directions of the scattered and incident radiations with respect to the rare-earth ion coordinates. To adapt their results to rare-earth garnets, three additional aspects must be considered. First, the unit cell contains six inequivalent rare-earth sites, and thus the Raman intensities from each must be appropriately summed. This requires a decomposition of the incident and scattered polarizations along the local axes of the different sites. Second, the crystal field interaction causes mixing of the Russell-Saunders wave function and thus the Raman tensor must deal with these mixed states. The appropriate wave functions for the electronic levels can be expressed as a linear combination of the Russell-Saunders wave functions

$$|\beta\rangle = \sum_{SLJJ_z} a_{SLJJ_z} |\gamma SLJJ_z\rangle \ . \tag{6}$$

The resulting Raman-scattering tensor for transitions between such levels β and β' is then given by[26]

$$(\alpha_{\rho\sigma})_{\beta'\beta} = \langle\beta'|\ \alpha_{\rho\sigma}|\ \beta\rangle$$
$$= \sum a^*_{SL'J'J'_z} a_{SLJJ_z} \langle\gamma' SL'J'J'_z|\ \alpha_{\rho\sigma}\ |\gamma SLJJ_z\rangle \ . \tag{7}$$

Since the mixture coefficients a_{SLJJ_z} are a result of the crystal field interaction, the relative Raman intensities for the different transitions might be used as a test of the crystal field parameters, similar to the use of g factors.[29] Third, for a rare-earth ion with an odd number of electrons (Kramer's ions), such as Dy^{3+}, the crystal field levels are all doubly degenerate. Thus, a given Raman transition from level β to β' will have four contributions to the scattering intensity, one from each of the four possible contributions.

As stated in Sec. III, in order to readily identify the symmetry of the *phonons*, the macroscopic axes of the dysprosium garnets were purposely oriented in a unique manner to the incident and scattered radiations, which were designated by *V-V*, *H-H*, *H-V*, and *V-H*. For these polarization combinations and this crystal orientation, the relative *electronic* Raman intensity contributions from all six inequivalent rare-earth sites add together to give (left-hand subscripts are scattered, right-hand subscripts are incident polarizations)

$$I_{(V\text{-}V)} \propto 2|\alpha_{\xi\xi}|^2 + |\alpha_{\eta\eta} + \alpha_{\xi\xi}|^2 + |\alpha_{\eta\xi} + \alpha_{\xi\eta}|^2 \ ,$$

$$I_{(H\text{-}H)} \propto \tfrac{1}{4}|\alpha_{\eta\eta} + \alpha_{\xi\xi} - 2\alpha_{\xi\xi} + \sqrt{2}\,(\alpha_{\xi\eta} - \alpha_{\eta\xi})|^2$$
$$+ \tfrac{1}{4}|\alpha_{\eta\xi} + \alpha_{\xi\eta} + \sqrt{2}\,(\alpha_{\xi\xi} - \alpha_{\xi\xi})|^2$$
$$+ |\alpha_{\eta\xi}|^2 + |\alpha_{\xi\eta}|^2 \ ,$$

$$I_{(H\text{-}V)} \propto \tfrac{1}{2}|\alpha_{\eta\eta} - \alpha_{\xi\xi} + \sqrt{2}\,\alpha_{\eta\xi}|^2 + \tfrac{1}{2}|\alpha_{\xi\eta} - \alpha_{\eta\xi} - \sqrt{2}\,\alpha_{\xi\eta}|^2$$
$$+ |\alpha_{\eta\xi}|^2 + |\alpha_{\xi\xi}|^2 \ ,$$

$$I_{(V\text{-}H)} \propto \tfrac{1}{2}|\alpha_{\eta\eta} - \alpha_{\xi\xi} - \sqrt{2}\,\alpha_{\eta\xi}|^2 + \tfrac{1}{2}|\alpha_{\xi\eta} - \alpha_{\eta\xi} - \sqrt{2}\,\alpha_{\eta\xi}|^2$$

TABLE IV. Comparison between observed and calculated crystal field levels (cm^{-1}).

Source of E_0	Free-ion assignment	DyAlG E_0(obs)	DyAlG E_c(calc)	DyAlG $E_0 - E_c$	DyGaG E_0 (obs)	DyGaG E_c(calc)	DyGaG $E_0 - E_c$
Ref. 11	$^6F_{1/2}$	13481.3	13481.8	−0.5	• • •	13422.8	• • •
Ref. 10	$^6F_{3/2}$	13379.0	13382.7	−3.7	13318.7	13313.5	5.2
		13372.0	13368.1	3.9	13308.5	13304.3	4.2
	$^6F_{5/2}$	12683.0	12680.4	2.6	12619.8	12606.5	13.3
		12538.0	12534.0	4.0	12475.5	12475.9	−0.4
		12507.0	12513.5	−6.5	12451.8	12460.0	−8.2
	$^6F_{7/2}$	11321.0	11317.8	3.2	11241.0	11233.2	7.8
		11279.0	11272.8	6.2	11210.0	11200.2	9.8
		11247.0	11251.5	−4.5	11191.0	11188.1	2.9
		11063.0	11067.8	−4.8	11008.0	11016.8	−8.8
	$^6H_{5/2}$	10515.0	10519.3	−4.3	10391.0	10391.8	−0.8
		10363.0	10363.9	−0.9	10343.0	10353.1	−10.1
		10257.0	10252.5	4.5	10225.0	10223.4	1.6
	$^6F_{9/2}$	9662.0	9667.3	−5.3	9563.0	9573.5	−10.5
	$^6H_{7/2}$	• • •	9412.3	• • •	9333.0	9338.1	−5.1
		9385.0	9404.0	−19.0	9310.0	9320.6	−10.6
		9349.0	9336.9	12.1	9287.0	9273.3	13.7
		9329.0	9327.0	2.0	9264.0	9256.8	7.2
		9321.0	9311.6	9.4	9255.0	9248.3	6.7
		9092.0	9103.6	−11.6	9026.0	9030.4	−4.4
		9057.0	9050.4	6.6	• • •	9025.6	• • •
		9022.0	9015.4	6.6	8986.0	8982.0	4.0
	$^6F_{11/2}$	8292.0	8294.1	−2.1	8161.0	8174.9	−13.9
	$^6H_{9/2}$	8223.0	8224.4	−1.4	8134.0	8139.6	−5.6
		8009.0	8008.5	0.5	7934.0	7933.6	0.4
		7983.0	7984.8	−1.8	7918.0	7908.8	9.2
		7958.0	7961.7	−3.7	7896.0	7892.9	3.1
		7927.0	7921.2	5.8	7875.0	7862.5	12.5
		7823.0	7826.1	−3.1	7751.0	7754.3	−3.3
		7780.0	7778.1	1.9	7724.0	7718.0	6.0
		7760.0	7752.6	7.4	7697.0	7692.5	4.5
		7684.0	7692.2	−8.2	7646.0	7646.9	−0.9
		7651.0	7645.8	5.2	7626.0	7621.5	4.5
	$^6H_{11/2}$	6132.0	6125.4	6.6	6042.0	6040.4	1.6
		6113.0	6106.7	6.3	6033.0	6032.9	0.1
		6062.0	6079.8	−17.8	6018.0	6015.2	2.8
		6040.0	6041.0	−1.0	5997.0	6001.7	−4.7
		5965.0	5957.2	7.8	5952.0	5950.8	1.2
		5938.0	5939.9	−1.9	5938.0	5945.7	−7.7
This work	$^6H_{13/2}$	3968.0	3962.9	5.1	3824.0	3826.5	−2.5
		3832.0	3823.7	8.3	3784.0	3792.4	−8.4
		3786.0	3781.1	4.9	3747.0	3745.9	1.1
		3719.0	3718.1	0.9	3647.0	3652.5	−5.5
		3673.0	3686.4	−13.4	3635.0	3640.4	−5.4
		3594.0	3598.4	−4.4	3576.0	3580.6	−4.6
		3565.0	3567.7	−2.7	3559.0	3562.7	−3.7
	$^6H_{15/2}$	• • •	763.9	• • •	• • •	576.3	• • •
		• • •	528.2	• • •	• • •	493.2	• • •
		• • •	491.3	• • •	• • •	455.0	• • •
		• • •	230.0	• • •	• • •	166.5	• • •
		186.0	179.2	6.8	137.0	133.8	3.2
		114.0	116.9	−2.9	70.0	76.1	−6.1
		69.0	63.6	5.4	21.0	25.1	−3.1
		0.0	0.0	0	0.0	0.0	0
Rms error				6.6			6.6

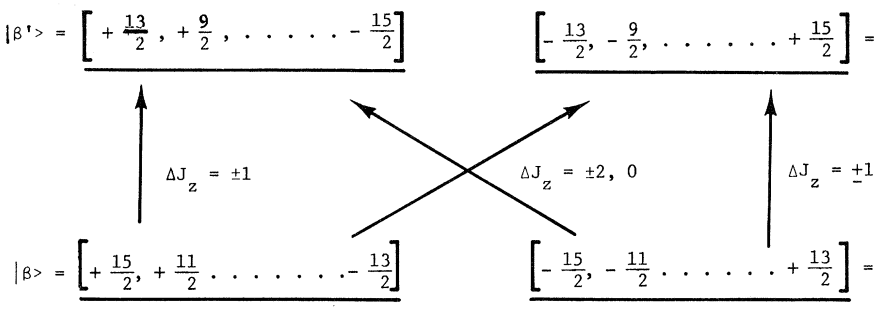

FIG. 5. Schematic diagram to illustrate the results of Table V b. Electronic Raman transitions from the initial Kramers doublet $|\beta\rangle$, $|\beta\rangle^*$ to the final Kramers doublet $|\beta'\rangle$, $|\beta'\rangle^*$ are shown. Numerals in brackets indicate possible J_z values mixed by D_2 crystal field. Contributions to the scattered intensity from the two $\Delta J_z = \pm 1$ transitions are equal, as are those of the two $\Delta J_z = 0, \pm 2$ transitions.

$$+ |\alpha_{\xi\eta}|^2 + |\alpha_{\xi\xi}|^2 . \quad (8)$$

The orientation of the local axes (η, ζ, ξ) for each of the six sites with respect to the macroscopic axes are clearly shown in Ref. 9. The subscripts (η, ζ, ξ) in these scattering tensors can now be thought of as (x, y, z) in the notations of Axe[25] and of Mortensen and Koningstein.[26] Recently Koningstein and Schaak,[30] in dealing with the summation over sites, preferred to rotate the electronic Raman-scattering tensor by rotational matrices into the six local sites. We, on the other hand, preferred to decompose the light polarizations into the local axis systems.

The relative intensities for the different polarization combinations, shown in Eq. (8), can be simplified conceptually if note is made of the following two facts: First, the electronic Raman transition connects states that differ by $\Delta J_z = \pm 2, \pm 1, 0$ due to the two-photon nature of this transition.[25,30,31] Second, the crystal field Hamiltonian with D_2 symmetry mixes only states whose J_z's differ by multiples of 2. Consequently, a given electronic Raman transition will involve either $\Delta J_z = 0, \pm 2$ or $\Delta J_z = \pm 1$, but not both. That is, we can separate the Raman intensities into two parts, as shown in Table V a. For calculation, the spherical tensorial form of the Raman tensor $\alpha_k^{(\lambda)}$ of Axe[25] is more convenient, and thus the results of Table V a are reexpressed in terms of $\alpha_k^{(\lambda)}$ in Table V b. The unitary transformation connecting the tensor components of $\alpha_k^{(\lambda)}$ and the Cartesian tensor components can be found in Ref. 32. One notes that $I_{V-H} = I_{H-V}$. Experimentally, this was confirmed for all transitions (see Table II).

An illustration of the latter two facts is shown in Fig. 5 for two Dy^{3+} levels described by Kramers ground states $|\beta\rangle$, $|\beta\rangle^*$ and Kramers excited state $|\beta'\rangle$, $|\beta'\rangle^*$. For simplicity, only the possible J_z quantum numbers are shown. The Raman intensity entails calculating the Raman-scattering-tensor components $\alpha_k^{(\lambda)}$ for transitions between $|\beta\rangle \rightarrow |\beta'\rangle$ $(\Delta J_z = \pm 1)$ and $|\beta\rangle \rightarrow |\beta'\rangle^* (\Delta J_z = \pm 2, 0)$. The transitions between $|\beta\rangle^* \rightarrow |\beta'\rangle^*$ and $|\beta\rangle^* \rightarrow |\beta'\rangle$ are identical, respectively, to the former two. The total electronic Raman intensity is then the summation of these four contributions.

In principle, we are now in the position to calculate the electronic Raman-scattering intensity for a given transition in DyAlG and DyGaG, once the polarization combination is specified. We can do this for the following reasons: The wave functions, expressed as a linear combination of 54 Russell-Saunders wave functions ($^6H_{15/2}$ to $^6F_{1/2}$), for each of the crystal field levels are known as a result of the best-fit determination of the crystal field parameters and free-ion energies (see Sec. IV); the contributions from each of the six rare-earth sites have been appropriately summed, and the results are given in Table V b; the contributions from Kramers levels can be readily summed as in Table V b (see also Fig. 5). However, one still needs to know the matrix elements $(4f|\hat{r}|n'l \pm 1)$ and the energies $\hbar\omega_{(n'l\pm1)}$ for all excited configurations. Even when Axe's[25] approximations on the

TABLE V. Relative intensities for all polarization combinations in terms of the scattering tensors: a—in Cartesian components, b—in spherical tensor components. Contributions from all the inequivalent sites have been added. Kramers doublet contributions are grouped separately (see Fig. 5).

	$\Delta J_z = \pm 1$	$\Delta J_z = 0, \pm 2$
		a
VV	0	$+ 2\lvert\alpha_{\xi\xi}\rvert^2 + \lvert\alpha_{\eta\eta} + \alpha_{\xi\xi}\rvert^2 + \lvert\alpha_{\eta\zeta} + \alpha_{\xi\eta}\rvert^2$
HH	$\frac{1}{2}\lvert\alpha_{\xi\eta} - \alpha_{\eta\zeta}\rvert^2 + \frac{1}{2}\lvert\alpha_{\xi\xi} - \alpha_{\xi\zeta}\rvert^2$	$+ \frac{1}{4}\lvert\alpha_{\eta\eta} + \alpha_{\xi\xi} - 2\alpha_{\zeta\zeta}\rvert^2 + \frac{1}{4}\lvert\alpha_{\xi\eta} + \alpha_{\eta\zeta}\rvert^2 + \lvert\alpha_{\eta\zeta}\rvert^2 + \lvert\alpha_{\xi\eta}\rvert^2$
HV = VH	$\lvert\alpha_{\xi\eta}\rvert^2 + \lvert\alpha_{\xi\xi}\rvert^2 + \lvert\alpha_{\eta\zeta}\rvert^2 + \lvert\alpha_{\xi\zeta}\rvert^2$	$+ \frac{1}{2}\lvert\alpha_{\eta\eta} - \alpha_{\xi\xi}\rvert^2 + \frac{1}{2}\lvert\alpha_{\xi\eta} - \alpha_{\eta\zeta}\rvert^2$
		b
VV	0	$+ 2(\alpha_0^2)^2 + (\alpha_2^2 - \alpha_{-2}^2)^2$
HH	$(\alpha_1^1)^2 + (\alpha_{-1}^1)^2$	$+ (\alpha_0^1)^2 + \frac{3}{2}(\alpha_0^2)^2 + \frac{3}{4}(\alpha_2^2 - \alpha_{-2}^2)^2$
HV = VH	$(\alpha_1^1)^2 + (\alpha_{-1}^1)^2 + (\alpha_1^2)^2 + (\alpha_{-1}^2)^2$	$+ (\alpha_0^1)^2 + \frac{1}{2}(\alpha_2^2 + \alpha_{-2}^2)^2$

TABLE VI. Comparison between calculated and observed (in parentheses) relative electronic Raman intensities for DyAlG. Calculated values are normalized to the observed I_{H-V} of assignment 1.

Assignments	I_{V-V}	I_{H-H}	I_{V-H}	I_{H-V}
6′	0.032 (· · ·)	0.026 (· · ·)	0.026 (0.010)	0.026 (0.008)
5′	0.013 (0.046)	0.011 (0.050)	0.074 (0.050)	0.074 (0.048)
4′	0.018 (0.040)	0.013 (0.033)	0.076 (0.057)	0.076 (0.054)
3′	0.011 (0.089)	0.010 (0.058)	0.016 (0.065)	0.016 (0.068)
2′	0.043 (0.046)	0.032 (0.027)	0.074 (0.088)	0.074 (0.088)
1′	0.712 (0.217)	0.537 (0.155)	0.124 (0.357)	0.124 (0.375)
0′	0.002 (0.009)	0.031 (0.088)	0.637 (0.760)	0.637 (0.760)
7	0.032 (· · ·)	0.024 (· · ·)	0.029 (· · ·)	0.029 (· · ·)
6	0.013 (· · ·)	0.014 (· · ·)	0.241 (· · ·)	0.241 (· · ·)
5	0.203 (· · ·)	0.154 (· · ·)	0.050 (· · ·)	0.050 (· · ·)
4	0.465 (· · ·)	0.357 (· · ·)	0.064 (· · ·)	0.064 (· · ·)
3	0.021 (0.05)	0.032 (0.08)	0.352 (0.08)	0.352 (0.08)
2	1.651 (1.7)	1.247 (1.3)	0.243 (0.80)	0.243 (0.80)
1	0.188 (0.15)	0.254 (0.85)	2.0 (2.0)	2.0 (2.0)

sums over configurations are used, one still needs to know the values for $(4f|r^2|4f)$ and $(4f|r|5d)^2$ and for $\hbar\omega_{5g}$ and $\hbar\omega_{5d}$. We follow Judd's[27] procedure of linear interpolation between Rajnak's[33] values for the radial functions, getting $(4f|r^2|4f) = 0.972$ a.u.^{2} and $(4f|r|5d) = 0.678$ a.u. We have used Dieke's[21] estimations for the energies, getting $\omega_{5g} \sim \omega_{\text{ionization}} = 197\,000$ cm^{-1} and $\omega_{5d} = 135\,000$ cm^{-1}. Using these values, we have calculated the relative Raman intensities for transitions originating from the ground state of DyAlG to the levels of the first and second manifolds. This was done for all four polarization combinations.

The calculated relative intensities are listed along with the observed data in Table VI. Only qualitative agreement between these two sets of intensities is found. To overcome the uncertainties in the radial matrix elements and the effective energies for the excited configurations, one might wish to treat these four values as adjustable parameters, as was the case for the nine crystal field parameters and free-ion energies. That is, besides solving for the best fit between the calculated and measured energies for the crystal field levels, one might simulataneously achieve the best-fit to the relative Raman intensities for the different polarization combinations. This procedure is planned for our recent data on YbAlG.[34]

VI. CONCLUSION

We have determined both the frequencies and symmetries of all except one of the 25 Raman-active phonons in DyAlG and DyGaG. Our particular choice of crystal orientation with respect to the incident and scattered polarization greatly facilitated the symmetry determination of these phonons. Our new assignments on the crystal field levels of $^6H_{15/2}$ and $^6H_{13/2}$ manifolds along with the previous assignments for other higher manifolds, motivated a complete crystal field analysis. The nine crystal field parameters for DyAlG and DyGaG were determined and for the first time these can be compared with the dilute salts of YAlG(Dy) and YGaG(Dy). We have found simple expressions for the relative electronic Raman-scattering intensity from all the six inequivalent rare-earth ion sites and appropriate for all different polarization combinations. In addition, the results of our crystal field analysis were applied to these simple expressions to calculate the relative Raman intensities for DyAlG. When these calculated intensities are compared with the observed intensities, qualitative agreement is definitely found. We suggest that in order to improve the agreement, the unknown radial matrix elements (two in all) and excited configuration energies (two in all) could be used as adjustable parameters, similar to the crystal field parameters and the free-ion energies in the crystal field best-fit analysis. The relative Raman intensities depend on the mixture coefficients of the eigenfunctions to the same order as the g factors. Thus, the Raman intensities may, in principle, serve the same role as the g factors in providing a good test for the crystal field analysis.

ACKNOWLEDGMENTS

We particularly wish to thank Stanley Mroczkowski of Yale University for the DyAlG and Barbara Wanklyn of Oxford University for the DyGaG. These large flux-grown crystals of excellent optical quality facilitated our measurements. We also wish to express our appreciation to G. M. Copland of Queen Mary College, London, and to W. P. Wolf and R. L. Cone of Yale University for several helpful discussions regarding the crystal field analysis, the computer program, and the orientations of local axes.

*Work supported by AFOSR under Grant No. F44620-69-C-0102, and by NSF under Grant No. GK-12509.

†Present address: IBM Thomas J. Watson Research Center, Yorktown Heights, N. Y. 10598.

[1]G. Menzer, Z. Krist. 63, 157 (1926).

[2]*The Irreducible Representations of Space Groups*, edited by J. Zak (Benjamin, New York, 1969).

[3]N. T. McDevitt, J. Opt. Soc. Am. 59, 1240 (1969).

[4]J. P. Hurrell, S. P. S. Porto, I. F. Chang, S. S. Mitra, and R. P. Bauman, Phys. Rev. 173, 851 (1968).

[5]G. Mace, G. Schaack, Toaning Ng, and J. A. Koningstein, Z. Physik 230, 391 (1970).

[6]J. E. Geusic, M. L. Hansel, and R. G. Smith, Appl. Phys. Letters 6, 175 (1965).

[7]C. F. Johnson, J. E. Geusic, and C. G. Van Uitert, Appl. Phys. Letters 7, 127 (1965).

[8]H. Van Vleck, J. Phys. Chem. Solids 27, 1047 (1966). This paper summarizes all the literature up to 1966.

[9]W. P. Wolf, *Proceedings of the International Conference on Magnetism, Nottingham, England*, 1964 (The

Institute of Physics and The Physical Society, London, 1965), p. 555.
[10]P. Grünberg, S. Hüfner, E. Orlich, and J. Schmitt, Phys. Rev. 184, 285 (1969).
[11]K. Aoyagi, K. Tsushima, and M. Uesugi, J. Phys. Soc. Japan 27, 49 (1969).
[12]R. A. Buchanan, K. A. Wickersheim, J. J. Pearson, and G. F. Herrmann, Phys. Rev. 159, 245 (1967); 159, 251 (1967).
[13]D. A. Huchital and J. Dane Rigden, Rev. Sci. Instr. 39, 1472 (1968).
[14]We wish to thank Dr. P. J. Kindlmann of Yale University for the design and construction of the digital photon counter.
[15]H. Winston and R. S. Halford, J. Chem. Phys. 17, 607 (1949).
[16]R. Loudon, Advan. Phys. 13, 423 (1964).
[17]M. Veyssie and B. Dreyfus, J. Phys. Chem. Solids 28, 499 (1967).
[18]R. J. Elliott and R. Loudon, Phys. Letters 3, 189 (1963).
[19]J. A. Koningstein and Toaning Ng, Solid State Commun. 7, 351 (1969).
[20]K. W. H. Stevens, Proc. Roy. Phys. Soc. (London) A65, 209 (1952).
[21]G. H. Dieke, *Spectra and Energy Levels of Rare Earth Ions in Crystals* (Interscience, New York, 1968).
[22]C. W. Nielson and G. F. Koster, *Spectroscopic Coefficients for the p^n, d^n, and f^n Configurations* (MIT, Cambridge, Mass., 1964).
[23]M. J. D. Powell, Computer J. 7, 303 (1965); Harwell Subroutine Library Program No. VA02A.
[24]B. G. Wybourne, J. Chem. Phys. 36, 2301 (1962).
[25]J. D. Axe, Jr., Phys. Rev. 136, A42 (1964).
[26]O. Sonnich Mortensen and J. A. Koningstein, J. Chem. Phys. 48, 3941 (1968).
[27]B. R. Judd, Phys. Rev. 127, 750 (1962).
[28]G. S. Ofelt, J. Chem. Phys. 37, 511 (1962).
[29]M. T. Hutchings and W. P. Wolf, J. Chem. Phys. 41, 617 (1964).
[30]J. A. Koningstein and G. Schaak, Phys. Rev. B 2, 1242 (1970).
[31]A. Kiel and S. P. S. Porto, J. Mol. Spectry. 32, 458 (1969).
[32]J. A. Koningstein and O. S. Mortensen, Phys. Rev. 168, 75 (1968).
[33]K. Rajnak, J. Chem. Phys. 37, 2440 (1962).
[34]B. E. Argyle, R. L. Wadsack, and R. K. Chang, 42, 1478 (1971).

PHYSICAL REVIEW B VOLUME 3, NUMBER 12 15 JUNE 1971

Thermal Expansion of Rocksalt*

B. N. N. Achar† and G. R. Barsch
Materials Research Laboratory and Department of Physics, The Pennsylvania State University, University Park, Pennsylvania 16802
(Received 5 November 1970)

The microscopic Grueneisen parameters and the temperature dependence of the thermal Grueneisen parameter of NaCl are calculated from a shell model with six parameters, five of which are taken as pressure dependent. All parameters are determined from experimental elastic, optical, and dielectric data at absolute-zero temperature. The results agree within 6–8% with experimental data. The discrepancy is primarily attributed to the experimental error of the input data that are used to determine the parameters of the model. Calculations have also been made for two versions of the rigid-ion model (RIM) which indicate that the apparent success previously attributed to the Kellermann model is mainly due to cancellation of errors arising from omitting second-nearest-neighbor interaction and electronic polarizability.

I. INTRODUCTION

While the caloric equation of state and the temperature dependence of the Debye temperature for NaCl have been extensively studied theoretically on the basis of the rigid-ion model (RIM) of Kellermann[1,2] as well as several versions of the shell model[3–6] (SM), for the thermal equation of state and the temperature dependence of the Grueneisen parameter γ, the only theoretical calculations available are based on the RIM.[7–13] Moreover, the results of Arenstein *et al.*[10] which are the only theoretical data for the temperature dependence of the Grueneisen parameter of NaCl are based on a dubious procedure of determining the two repulsive parameters for the nearest-neighbor short-range interaction. These authors prefer to determine the repulsive parameters from the bulk modulus and the TO frequency and ignore the equilibrium condition. The results refer to a series of different values for the interatomic distance, and the quality of agreement with experimental data depends on the proper choice of one of these values. These "values have been corrected to the actual lattice spacing at each temperature" by Meincke and Graham[11] who find that the general shape of the γ vs T curve shows a minimum near 11 °K and agrees qualitatively very well with their own experimental values, but that